processes

MDPI

Article

Catalytic Ozonation of Nitrite in Denitrification Wastewater Based on Mn/ZSM-5 Zeolites: Catalytic Performance and Mechanism

Yiwei Zhang [1], Yulin Sun [1], Yanqun Zhu [1,2,*], Wubin Weng [1,2], Yong He [1,2] and Zhihua Wang [1,2,*]

[1] State Key Laboratory of Clean Energy Utilization, Zhejiang University, Hangzhou 310027, China; yiwei_zhang@zju.edu.cn (Y.Z.); sunyulin@zju.edu.cn (Y.S.); wengwubin@zju.edu.cn (W.W.); heyong@zju.edu.cn (Y.H.)
[2] Qingshanhu Energy Research Center, Zhejiang University, Hangzhou 311300, China
* Correspondence: yqzhu@zju.edu.cn (Y.Z.); wangzh@zju.edu.cn (Z.W.)

Abstract

In wet flue gas desulfurization and denitrification processes, nitrite accumulation inhibits denitrification efficiency and induces secondary pollution due to its acidic disproportionation. This study developed a Mn-modified ZSM-5 zeolite catalyst, achieving efficient resource conversion of nitrite in nitrogen-containing wastewater through an O_3 + Mn/ZSM-5 catalytic system. Mn/ZSM-5 catalysts with varying SiO_2/Al_2O_3 ratios (prepared by wet impregnation) were characterized by BET, XRD, and XPS. Experimental results demonstrated that Mn/ZSM-5 (SiO_2/Al_2O_3 = 400) exhibited a larger specific surface area, enhanced adsorption capacity, abundant surface Mn^{3+}/Mn^{4+} species, hydroxyl oxygen species, and chemisorbed oxygen, leading to superior oxidation capability and catalytic activity. Under the optimized conditions of reaction temperature = 40 °C, initial pH = 4, Mn/ZSM-5 dosage = 1 g/L, and O_3 concentration = 100 ppm, the NO_2^- oxidation efficiency reached 94.33%. Repeated tests confirmed that the Mn/ZSM-5 catalyst exhibited excellent stability and wide operational adaptability. The synergistic effect between Mn species and the zeolite support significantly improved ozone utilization efficiency. The O_3 + Mn/ZSM-5 system required less ozone while maintaining high oxidation efficiency, demonstrating better cost-effectiveness. Mechanism studies revealed that the conversion pathway of NO_2^- followed a dual-path catalytic mechanism combining direct ozonation and free radical chain reactions. Practical spray tests confirmed that coupling the Mn/ZSM-5 system with ozone oxidation flue gas denitrification achieved over 95% removal of liquid-phase NO_2^- byproducts without compromising the synergistic removal efficiency of NO_x/SO_2. This study provided an efficient catalytic solution for industrial wastewater treatment and the resource utilization of flue gas denitrification byproducts.

Keywords: nitrite; ozone; catalytic ozonation; Mn/ZSM-5 zeolite; byproducts treatment; resource utilization

Academic Editor: Giancarlo Cravotto

Received: 4 July 2025
Revised: 20 July 2025
Accepted: 25 July 2025
Published: 27 July 2025

Citation: Zhang, Y.; Sun, Y.; Zhu, Y.; Weng, W.; He, Y.; Wang, Z. Catalytic Ozonation of Nitrite in Denitrification Wastewater Based on Mn/ZSM-5 Zeolites: Catalytic Performance and Mechanism. *Processes* **2025**, *13*, 2387. https://doi.org/10.3390/pr13082387

1. Introduction

Nitrogen oxides (NO_x), as one of the primary atmospheric pollutants, not only contribute to the formation of photochemical smog [1], haze [2], and acid rain [3] but also pose significant risks to the human respiratory system [4]. In recent years, low-temperature oxidation flue gas denitrification technology using ozone has been widely adopted in boilers, kilns, and non-power industries due to its high efficiency, broad applicability, and

capability for synergistic multi-pollutant control [5,6]. This technology uses the strong oxidative capacity of ozone to convert poorly soluble NO in flue gas into higher-valence species (e.g., NO_2, NO_3, N_2O_5) [7,8], oxidize Hg^0 to Hg^{2+} [9], and degrade VOCs into CO_2 and H_2O [10]. Coupled with a wet scrubbing process, it enables integrated removal of multiple pollutants [11]. In wet flue gas treatment systems, the primary absorption products of NO_x are nitrite (NO_2^-) and nitrate (NO_3^-) [12–14]. While nitrates are chemically stable and serve as key raw materials for construction, fertilizers, and phase-change materials [15–17], liquid-phase NO_2^- is unstable and prone to disproportionation reactions under acidic conditions, releasing NO back into the atmosphere and causing secondary pollution [18]. Moreover, high concentrations of NO_2^- in the absorbent slurry inhibit NO_x absorption, reducing denitrification efficiency. The accumulation of NO_2^- also necessitates frequent replacement of industrial water, exacerbating water resource wastage. Additionally, NO_2^- itself is highly toxic, and its excessive emission poses severe threats to ecosystems and human health [19,20]. Therefore, developing cost-effective methods for NO_2^- removal or its resource recovery is critical for the large-scale application of ozone oxidation flue gas denitrification technology and wet process technology in industrial settings [11,21].

A variety of physical, chemical, and biological methods have been employed for pollutant removal from water [22,23]. Among these, physical adsorption has been preferentially adopted for nitrite elimination in industrial wastewater treatment, with typical adsorbents including activated carbon [24] and reverse osmosis membranes [25,26]. However, this technology suffers from inherent limitations such as insufficient adsorption selectivity, susceptibility to micropore clogging, and constraints in absorption tower modifications. These drawbacks directly lead to declining NO_2^- removal efficiency and increased operational costs. Current wastewater treatment systems also encompass diversified approaches, including catalytic reduction [27,28], γ-ray irradiation [29], and ion exchange [30]. Nevertheless, the requirements for precious metal catalysts and complex equipment configurations make them poorly compatible with the engineering demands of wet scrubbing processes. Aerobic denitrification technology [31,32] has emerged as a novel biological nitrogen removal strategy, where denitrifying bacteria metabolically convert nitrite into N_2. However, this method typically requires prolonged treatment durations, and its temperature-sensitive nature presents significant compatibility challenges with the slurry environment in wet scrubbing processes, thereby limiting its practical application.

Based on the above comprehensive analysis, current nitrite treatment technologies are generally constrained by slow reaction kinetics, high operational costs, and stringent reaction requirements, making them incompatible with wet spray systems. In contrast, heterogeneous wet catalytic oxidation technology enables precise regulation of reaction pathways through the construction of efficient catalytic systems [33–35], while facilitating the conversion of nitrite to nitrate, thereby achieving resource utilization of pollutants. Regarding oxidants, ozone oxidation has remained a research focus in the advanced oxidation area due to its strong oxidative capacity [36,37]. Building upon this, the heterogeneous wet catalytic ozonation system has been successfully applied for deep mineralization of typical pollutants, including pharmaceuticals, pesticides, dyes, aromatic hydrocarbons, and organic acids, with commonly used catalysts such as activated carbon [38], TiO_2 [39], and Al_2O_3 [40]. However, radical-dominated advanced oxidation mechanisms generally suffer from a lack of reaction selectivity and are prone to competitive reaction interference, leading to significant degradation efficiency reduction for target pollutants [41]. Therefore, comprehensive consideration is required for catalyst selection. SiO_2-supported catalysts exhibit superior dispersion of active metal particles [42], but anomalous phenomena occurring during the reaction process, including carbon deposition, sintering of active metals, and structural loss of the SiO_2 support, can lead to the degradation of the active metal/SiO_2

architecture, thereby accelerating catalyst deactivation [43]. HZSM-5 zeolite has demonstrated potential in catalytic applications due to its high specific surface area, tunable acid sites, and well-defined pore structure [44–46]. Moreover, HZSM-5 exhibits properties such as easy handling, strong thermal stability, acid resistance, and recyclability, making it an ideal catalyst support [47]. However, its narrow channels hinder reactant/product diffusion [48–50], thereby constraining its selective oxidation capability toward NO_2^-. Meanwhile, Mn-based catalysts often demonstrate excellent catalytic oxidation performance through modulation of surface acidity and oxygen vacancy density [51,52]. During ozonation processes, Mn loading on catalysts can enhance ozone decomposition capacity and optimize reaction pathways by constructing redox-active centers [53–55]. Existing studies have also revealed that synergistic effects between Mn species and zeolite supports can form bifunctional catalytic interfaces, simultaneously promoting oxidant activation and target pollutant adsorption [56–58].

In response to the technical challenges in current nitrite removal processes, this study developed an innovative O_3 + Mn/ZSM-5 heterogeneous wet catalytic oxidation system. The tailored design of Mn/ZSM-5 catalysts with controlled SiO_2/Al_2O_3 ratios (fabricated via wet impregnation) demonstrated exceptional NO_2^- oxidation performance, with the Mn/ZSM-5 structure–activity correlations and NO_2^- conversion pathways systematically unraveled through kinetic studies and multi-technique characterizations. The catalyst's stability and potential for engineering applications were further validated. This work provided technical support for the resource utilization of nitrogen-containing wastewater and the green upgrading of wet flue gas desulfurization/denitrification processes.

2. Experiment and Methodology

2.1. Materials and Reagents

The HZSM-5 zeolites used in this work were supplied by Xfnano technology Co., Ltd. (Nanjing, China). Manganese nitrate (50% in H_2O, $Mn(NO_3)_2$), ethanol (≥99.5%, C_2H_6O), sodium nitrite (≥99.0%, $NaNO_2$), phosphoric acid (≥85.0%, H_3PO_4), and sodium hydroxide (≥96.0%, NaOH) were purchased from Sinopharm Chemical Reagent Co., Ltd. (Shanghai, China). Nitrogen gas (99.999%, N_2) and oxygen gas (99.999%, O_2) were supplied by Jingong Material Co., Ltd. (Hangzhou, China). All chemicals were procured from commercial suppliers and were used directly in this study without further purification.

2.2. Catalyst Preparation

Mn-modified ZSM-5 zeolite catalysts with different SiO_2/Al_2O_3 ratios were synthesized through a wet impregnation approach. The detailed preparation procedure was as follows: 2.0 g of HZSM-5 zeolite support was precisely weighed and transferred into a 100 mL beaker. Subsequently, 20 mL of anhydrous ethanol was added, followed by the addition of manganese nitrate corresponding to a 5 wt% Mn loading (10.589 g $Mn(NO_3)_2$ solution). The mixture was magnetically stirred in a water bath maintained at 40 °C until complete evaporation of the ethanol solvent. The resulting solid was dried at 105 °C for 12 h, followed by calcination in a muffle furnace at 400 °C for 4 h to obtain the final Mn/ZSM-5 catalysts with different SiO_2/Al_2O_3 ratios. The metal loading and SiO_2/Al_2O_3 ratios of the prepared catalysts were quantitatively analyzed by ICP-OES, as presented in Table 1. All five catalysts exhibited consistent Mn loadings of approximately 5 wt%, with measured SiO_2/Al_2O_3 ratios of 21.2, 85.3, 200.1, 300.0, and 399.6, respectively. These values showed excellent agreement with the predetermined specifications, confirming the successful preparation of the target catalysts.

Table 1. The metal loading and SiO_2/Al_2O_3 ratios of the prepared catalysts.

Catalysts	Actual SiO_2/Al_2O_3	Loaded Metal	Actual Mn Content
HZSM-5 (400)	400.1	-	0
Mn/ZSM-5 (21)	21.2	Mn	5.06 wt%
Mn/ZSM-5 (85)	85.3	Mn	5.11 wt%
Mn/ZSM-5 (200)	200.1	Mn	4.99 wt%
Mn/ZSM-5 (300)	300.0	Mn	5.04 wt%
Mn/ZSM-5 (400)	399.6	Mn	5.01 wt%

2.3. Catalytic Activity Tests

This study established an ozone-assisted heterogeneous wet catalytic oxidation system, as illustrated in Figure 1. The structure–performance relationship of the catalysts was precisely modulated by controlling two critical factors: the framework SiO_2/Al_2O_3 ratio of ZSM-5 zeolite and the loading of active metal species. Furthermore, the reaction kinetic characteristics were thoroughly analyzed by examining the coupling effects between ozone mass transfer efficiency and key thermodynamic parameters.

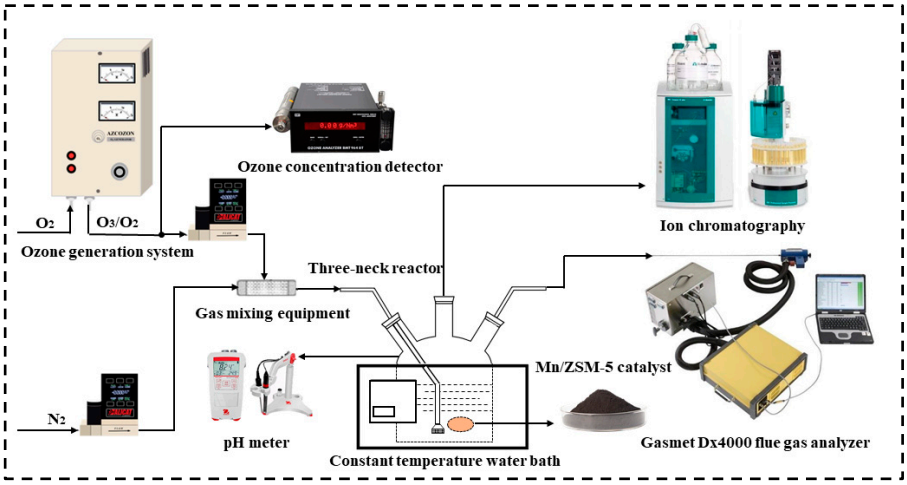

Figure 1. Ozone-assisted heterogeneous wet catalytic oxidation system schematic.

All gas streams in the system were precisely regulated using mass flow controllers (ALICAT, Tucson, AZ, USA). Ozone was generated by an ozone generator (AZCOZON-HTU500, Vancouver, BC, Canada) and subsequently divided into two pathways. The O_3/O_2 stream was directed to an ozone analyzer (BMT-964BT, Filderstadt, Germany) for real-time monitoring of ozone concentration. Based on calculation results, the O_3/O_2 stream was introduced as the reaction gas into a gas-mixing equipment. The mixed gas was introduced into the liquid phase via a fine bubble diffuser to facilitate the reaction. Sodium nitrite was employed as the source of NO_2^- in the aqueous phase. The reaction solution, containing predetermined amounts of catalyst, was maintained in the reactor with continuous pH monitoring using a digital pH meter (OHAUS-ST3100, Parsippany, NJ, USA). Temperature control was achieved through a circulating thermostatic water bath (Aohua HH-S, Changzhou, China). The exhaust gas from the reaction system passed through a pretreatment unit before being analyzed by a Fourier-transform infrared gas analyzer (Gasmet Dx4000, Helsinki, Finland) for compositional quantification. Concentrations of NO_2^- and NO_3^- were determined by ion chromatography (Metrohm 930, Herisau, Switzerland).

In addition to oxidation reactions, the disproportionation reaction of NO_2^- under acidic conditions must also be considered (Equation (1)):

$$3NO_2^- + 2H^+ = 2NO \uparrow + NO_3^- + H_2O \quad (1)$$

The conversion efficiency of NO_2^- considering both oxidation and disproportionation reactions can be calculated using the following formula:

$$\left[NO_2^-\right]_{con.} = \frac{c_{initial}\left(NO_2^-\right) - c\left(NO_2^-\right)}{c_{initial}\left(NO_2^-\right)} \times 100\% \quad (2)$$

$$\left[NO_2^-\right]_{con.O} = \frac{69 \times \left(c\left(NO_3^-\right) - c_{initial}\left(NO_3^-\right)\right) - 31 \times \left(c_{initial}\left(NO_2^-\right) - c\left(NO_2^-\right)\right)}{62 \times c_{initial}\left(NO_2^-\right)} \times 100\% \quad (3)$$

$$\left[NO_2^-\right]_{con.D} = \frac{93 \times \left(c_{initial}\left(NO_2^-\right) - c\left(NO_2^-\right)\right) - 69 \times \left(c\left(NO_3^-\right) - c_{initial}\left(NO_3^-\right)\right)}{46 \times c_{initial}\left(NO_2^-\right)} \times 100\% \quad (4)$$

where $\left[NO_2^-\right]_{con.}$, $\left[NO_2^-\right]_{con.O}$, $\left[NO_2^-\right]_{con.D}$ are the total conversion efficiency of NO_2^-, conversion efficiency via oxidation reaction, and conversion efficiency via disproportionation reaction, respectively. $c_{initial}\left(NO_2^-\right)$, $c_{initial}\left(NO_3^-\right)$ are the initial concentration of NO_2^- and NO_3^- in the liquid phase, unit mg/L, respectively. $c\left(NO_2^-\right)$, $c\left(NO_3^-\right)$ are final concentration of NO_2^- and NO_3^- after reaction, unit mg/L, respectively.

The ozone oxidation flue gas pollutant coupling wet spray system is shown in Figure 2. A lab-scale spray tower was designed following industrial specifications. The impact of the O_3 + Mn/ZSM-5 catalytic system on NO_x/SO_2 removal efficiency in the flue gas and the scrubbing stability of the original system were investigated. The ozone generation and flue gas analysis procedures were consistent with those described for Figure 1. Simulated flue gas premixed with O_3 was introduced into a quartz cylindrical reactor (650 mm length × 50 mm inner diameter) housed in a tubular furnace (Yifeng YFK60×600/10QK-G, Shanghai, China) for oxidation. The scrubbing system comprised a spray tower (inner diameter: 76 mm), a gear pump, an absorbent slurry circulation system, and a slurry sampling and analysis unit. The system operated under controlled conditions: slurry temperature: 50 ± 0.5 °C (maintained by an electronically controlled system with triple-blade impeller and mixed-flow pump agitation) and pH: 5.5 ± 0.1 (monitored in real-time using a calibrated pH meter). The gear pump (Levu CT3001S, Baoding, China) delivered the absorbent slurry to a fine-atomization solid-cone nozzle within the tower. The absorbent slurry comprised 3 L phosphate buffer solution (Na_2HPO_4-NaH_2PO_4) and a predetermined dosage of Mn/ZSM-5 zeolite catalyst. The concentration dynamics of nitrite byproducts in the liquid phase were quantitatively monitored through the integrated sampling and analysis system.

Similarly, the removal efficiency of NO_2^- in the liquid phase can be calculated using Equations (2)–(4). The removal efficiency of NO_x ($\eta(NO_x)$) and SO_2 ($\eta(SO_2)$) in the flue gas are determined by the following formula:

$$\eta(NO_x) = \frac{c_{inlet}(NO_x) - c_{outlet}(NO_x)}{c_{inlet}(NO_x)} \times 100\% \quad (5)$$

$$\eta(SO_2) = \frac{c_{inlet}(SO_2) - c_{outlet}(SO_2)}{c_{inlet}(SO_2)} \times 100\% \quad (6)$$

where $c_{inlet}(NO_x)$, $c_{outlet}(NO_x)$ are the concentrations of NO_x at the system inlet and after spray absorption, unit mg/Nm^3, respectively. $c_{inlet}(SO_2)$, $c_{outlet}(SO_2)$ are the concentrations of SO_2 at the system inlet and after spray absorption, unit mg/Nm^3, respectively.

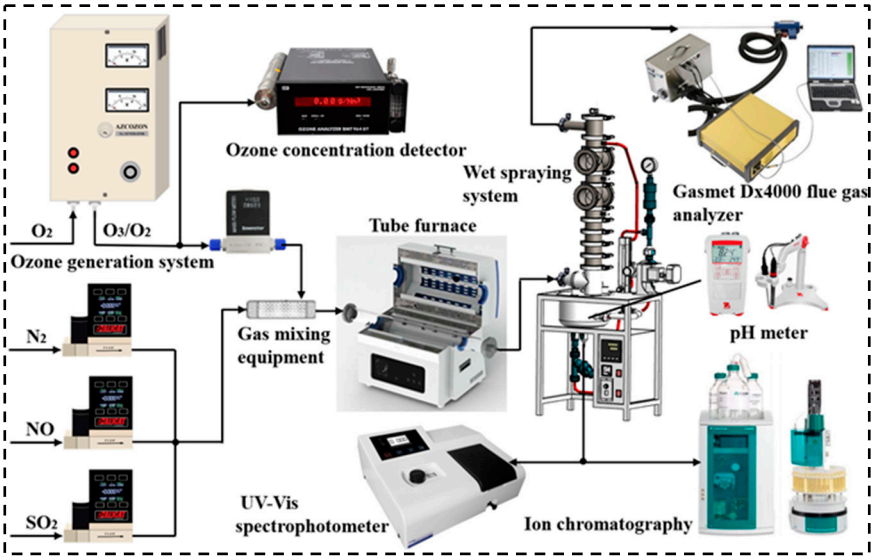

Figure 2. Ozone oxidation flue gas pollutant coupling wet spray system schematic.

2.4. Catalyst Characterization

After catalysts were pretreated at 200 °C in vacuum, the BET-specific surface area was measured by N_2 adsorption–desorption isotherms using an automatic surface area and porosity analyzer (Micromeritics ASAP 2460, Norcross, GA, USA) at 77 K. And the BJH method was used to calculate the pore volume and average pore diameter of catalysts. Elemental analysis (ICP-OES) was conducted on an inductively coupled plasma-optical emission spectrometer (Agilent 5110, Santa Clara, CA, USA). It was used for quantitative analysis of manganese loading and SiO_2/Al_2O_3 ratio in Mn/ZSM-5 catalysts. The X-ray diffraction (XRD) patterns of the catalysts were recorded by a Rigaku D/max 2550PC diffractometer (Rigaku, Tokyo, Japan) using monochromatized Cu Kα radiation (λ = 0.15406 nm), over a diffraction angle range of 10° to 80° at a scanning speed of 1°/min. The surface atomic chemical states were determined on an X-ray photoelectron spectrometer (Waltham, MA, USA) using a standard Al Kα source (1486.6 eV), and all the binding energies were referenced to the C 1s peak at 284.8 eV.

3. Results and Discussion

3.1. Relationship Between Catalytic Performance and Catalyst Properties

3.1.1. Effect of Zeolite SiO_2/Al_2O_3 on Catalytic Ozonation of NO_2^-

As shown in Figure 3, the catalytic oxidation performance of NO_2^- was significantly influenced by the SiO_2/Al_2O_3 ratios of the Mn/ZSM-5 zeolites. The physicochemical properties of ZSM-5 exhibit a distinct structure–activity relationship with its framework SiO_2/Al_2O_3 ratio, while the incorporation of transition metal Mn further modulates the distribution of active sites. To elucidate the intrinsic material characteristics governing NO_2^- conversion pathways in the liquid phase, the catalytic performance of Mn/ZSM-5 with varying SiO_2/Al_2O_3 ratios was systematically investigated. For clarity in subsequent discussion, the following terms were defined: NC is the total conversion efficiency of NO_2^-, NCO is the NO_2^- conversion efficiency attributed to the oxidation reaction, and NCD is the NO_2^- conversion efficiency resulting from the disproportionation reaction. Experimental results revealed that higher SiO_2/Al_2O_3 ratios enhanced oxidative reaction selectivity. At

SiO_2/Al_2O_3 = 400, the system achieved 97.3% total NO_2^- conversion efficiency with 96.95% contribution from the oxidative pathway.

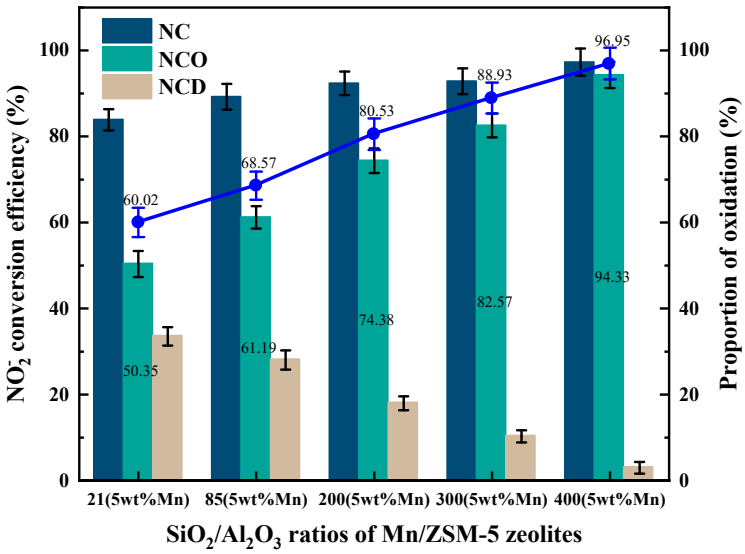

Figure 3. Effect of Mn/ZSM-5 zeolite SiO_2/Al_2O_3 on catalytic ozonation of NO_2^-.

3.1.2. Textual Properties

N_2 adsorption–desorption isotherms and the pore size distribution curves for Mn/ZSM-5 zeolites are shown in Figure S1, and Table S1 presents the textual properties of the catalysts. All the catalysts exhibited type IV isotherms with a H4 hysteresis loop [59], indicating the plentiful micropores and small mesopores. The pore size distributions of the five Mn/ZSM-5 catalysts were similar. The intensity of the curve was higher below 3 nm, and there was a small peak at 3.4–4.4 nm. This also indicated that the pores on the catalyst were mainly composed of abundant micropores and small mesopores, which was in line with the typical characteristics of zeolite catalysts. The BET surface areas for different catalysts ranked as follows: Mn/ZSM-5 (400) > Mn/ZSM-5 (300) > Mn/ZSM-5 (200) > Mn/ZSM-5 (85) > Mn/ZSM-5 (21). Results found that the specific surface area of zeolites increased significantly with the increase in the SiO_2/Al_2O_3 ratio. A higher BET surface area would produce more active sites for adsorption, activation, and oxidation, which would eventually contribute to the excellent catalytic performance of catalysts [60]. Among all the catalysts, Mn/ZSM-5 (400) had the largest surface area (398.9 $m^2 \cdot g^{-1}$) and pore volume (0.103 $cm^3 \cdot g^{-1}$), in accordance with its highest catalytic activity.

3.1.3. Crystalline Structures

The XRD patterns of various Mn/ZSM-5 zeolites are shown in Figure S2. All of the catalysts exhibited typical characteristic peaks at 13.8°, 14.8°, 23.1°, 23.3°, 23.9°, and 29.8°, corresponding to the (102), (112), (501), (051), (303), and (630) plane of ZSM-5 (JCPDS#42-0023) and HZSM-5 (JCPDS#49-0657) [61]. Results found that the strongest characteristic diffraction peaks of Mn/ZSM (21), Mn/ZSM (85), Mn/ZSM (200), Mn/ZSM (300), and Mn/ZSM (400) samples were at 23.09°, 23.06°, 23.02°, 23.03°, and 23.05°, respectively, which corresponded well with the (501) crystal plane in ZSM-5 (23.12°) and shifted slightly to the left. The strongest characteristic diffraction peak of HZSM-5 was at 22.99°. It showed that the strongest characteristic diffraction peaks of the Mn/ZSM-5 samples were all between those of ZSM-5 and HZSM-5. The reason was that the introduction of Mn caused the crystal plane spacing to become smaller, which also confirmed the loading and dispersion of Mn on the catalyst. In the five catalysts, no characteristic diffraction peaks corresponding to Mn species were found, indicating that Mn has excellent dispersion and weak crystallinity

on the zeolite carrier. The dispersed Mn species did not damage the skeleton structure, but instead filled or modified the zeolite support.

3.1.4. Surface Properties

The XPS analysis was used to characterize the oxidation states and distribution of surface species, and the results are shown in Figure S3. Furthermore, the quantitative ratios were calculated by deconvolution of XPS curves and presented in Table S2. The Mn $2p_{3/2}$ spectrum (shown in Figure S3a) exhibited three main peaks at ~643.3 eV, 641.9 eV, and 640.9 eV, which were assigned to Mn^{4+}, Mn^{3+}, and Mn^{2+}, respectively [62,63]. It could be seen that there were abundant species of Mn^{4+}, Mn^{3+}, and Mn^{2+} on all five Mn/ZSM-5 catalysts. It is noteworthy that the order of Mn^{3+} proportion was as follows: Mn/ZSM-5 (400) > Mn/ZSM-5 (300) > Mn/ZSM-5 (200) > Mn/ZSM-5 (85) > Mn/ZSM-5 (21), which was similar to the catalytic activity order. Mn^{3+} is generally believed to be closely related to the generation of oxygen vacancies, which can promote the decomposition of ozone and act as active sites for the ozonation [64–66].

Figure S3b presents the XPS spectra of O 1s, and the curves were deconvoluted into three peaks located at ~532.8 eV, 531.6 eV, and 529.9 eV, corresponding to hydroxyl oxygen species (O_{OH}), surface-adsorbed oxygen species (O_{ad}), and lattice oxygen species (O_{la}), respectively [10,67]. The detailed species ratios are listed in Table S2. Results found that there were abundant hydroxyl oxygen species and surface adsorbed oxygen species on the surface of the Mn/ZSM-5 catalyst, which was related to the high specific surface area and H_2O adsorption of the zeolite carrier. It was beneficial for the adsorption and conversion of reactants on oxygen vacancies [68,69]. The abundant surface hydroxyl species (O_{OH}) can timely convert the adsorbed NO_2^- on the catalyst into NO_3^-, improve the conversion rate and oxidation activity of NO_2^-, and reduce the selectivity of the disproportionation reaction. The density of O_{OH} on the heterogeneous catalytic surface was believed to be crucial for the initiation of ·OH from the decomposition of ozone [70]. In addition, surface adsorbed oxygen species (O_{ad}) were usually considered to be conducive to the formation of oxygen vacancies, which contributed to better catalytic performance [71,72]. As shown in Table S2, Mn/ZSM-5 (400) exhibited a significantly higher O_{OH} proportion compared to the other four samples, and it also had a rich O_{ad} proportion, which corresponds to its outstanding catalytic oxidation activity.

3.1.5. Adsorption Properties in Liquid Phase

The superior performance of high SiO_2/Al_2O_3 ratio Mn/ZSM-5 can be attributed to its key adsorption properties. Firstly, the higher zero charge point of Mn/ZSM-5 with an elevated SiO_2/Al_2O_3 ratio resulted in greater surface positive charges under acidic conditions, thereby enhancing NO_2^- adsorption capacity [73]. Secondly, there was a competitive adsorption relationship between ozone and water molecules on the surface of zeolites. Zeolites with a high SiO_2/Al_2O_3 ratio had strong hydrophobicity due to their high silicon content, which was more conducive to the adsorption of ozone on the surface [74,75], thereby promoting the contact between NO_2^- and active molecules.

3.2. Performance of O_3 + Mn/ZSM-5 System for Catalytic Oxidation of NO_2^-

As illustrated in Figure 4, significant differences were observed in the conversion pathways and efficiency of NO_2^- among different oxidation systems. In the 20% O_2 direct oxidation system, the total NO_2^- conversion efficiency reached only 49.9%. Pathway analysis revealed that 95.91% of this conversion originated from the self-disproportionation of nitrite, which is considered an undesirable side reaction. This finding confirms that oxygen alone is insufficient to drive the directional oxidation of liquid-phase NO_2^- effectively. To

enhance oxidation efficiency, an ozone-assisted catalytic system was developed. Experimental results demonstrated that O_3 participation increased the total NO_2^- conversion efficiency to 69.1%. However, the oxidative pathway contribution rate remained limited to 39.77%, indicating the need for further optimization to improve the selectivity toward the desired oxidation pathway.

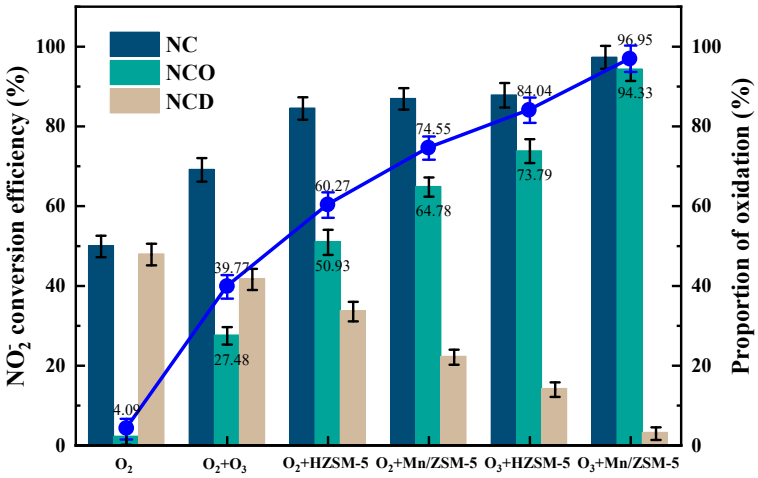

Figure 4. The conversion pathways and efficiency of NO_2^- among different oxidation systems.

To address this limitation, HZSM-5 zeolite was introduced to construct a heterogeneous catalytic system. When SiO_2/Al_2O_3 = 400, the O_2 + HZSM-5 system achieved a remarkable increase in total NO_2^- conversion efficiency to 84.5%, with the oxidation efficiency reaching 50.93% (approximately 24-fold higher than that of the pure O_2 system). This demonstrated that the HZSM-5 zeolite significantly enhanced the selectivity of the NO_2^- oxidation reaction while suppressing the disproportionation reaction. The improvement can be attributed to the HZSM-5 zeolite's adsorption capability for both free NO_2^- and O_2 in the liquid phase, thereby increasing their collision probability and promoting the oxidation of NO_2^- to NO_3^-. Further enhancement was observed upon introducing O_3, which elevated the NO_2^- oxidation efficiency from 50.93% (O_2 + HZSM-5) to 73.79% (O_3 + HZSM-5). As shown in Figure 4, the Mn/ZSM-5 catalyst exhibited superior performance in optimizing oxidative pathway selectivity while minimizing disproportionation. Under optimized conditions (T = 40 °C, $c_{initial}\left(NO_2^-\right)$ = 100 mg/L, Mn/ZSM-5 dosage = 1 g/L, SiO_2/Al_2O_3 = 400, O_3 = 100 ppm, O_2 = 20%, and initial pH = 4), O_3 + Mn/ZSM-5 system achieved 94.33% NO_2^- oxidation efficiency (NCO) and only 2.97% disproportionation conversion (NCD). This represents near-complete selectivity for the oxidative pathway, effectively eliminating secondary pollution concerns associated with byproduct utilization.

The cycling stability and structural durability of catalysts are critical metrics for evaluating their industrial applicability, as these properties directly determine process economics and environmental benefits. The recycling performance of the Mn/ZSM-5 zeolite catalyst is presented in Figure 5. Results found that the Mn/ZSM-5 catalyst demonstrated exceptional and stable catalytic activity across five consecutive experimental cycles. During the 15-h continuous operation, NO_2^- oxidation efficiency consistently exceeded 93%. Disproportionation reaction was effectively suppressed at a minimal level (<4%), and no detectable NO re-emission was observed. These results confirmed the outstanding reusability of Mn/ZSM-5, maintaining robust catalytic oxidation stability even under prolonged operation in acidic environments. The synergistic structure–performance stability endows Mn/ZSM-5 with significant industrial potential for high-concentration nitrite wastewater treatment.

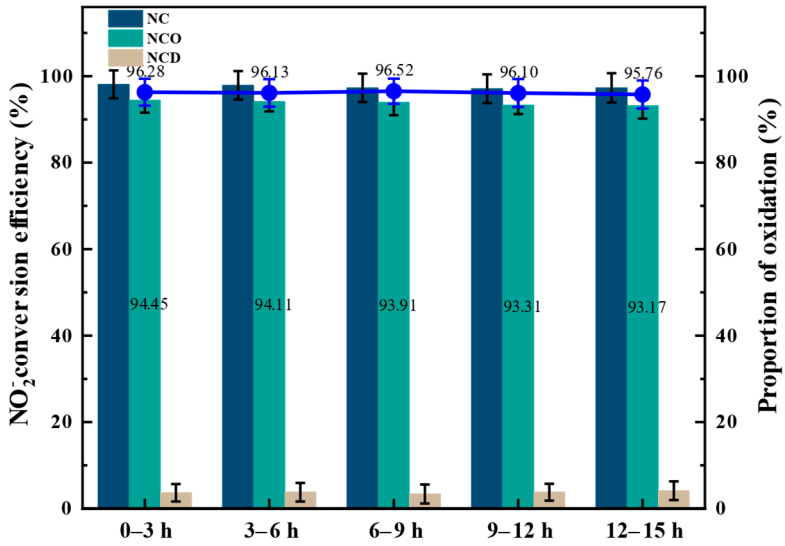

Figure 5. The recycling performance of Mn/ZSM-5 zeolite catalyst.

3.3. Effects of Different System Conditions on NO_2^- Oxidation Efficiency

3.3.1. Effect of Reaction Temperature

Temperature represents one of the most critical parameters in catalytic systems. Figure 6 illustrates the effect of reaction temperature on NO_2^- oxidation efficiency and conversion pathways in the ozone-assisted wet catalytic oxidation system. The results demonstrated that elevated temperatures adversely affected oxidation efficiency. In the O_3 + HZSM-5 system, NO_2^- oxidation efficiency decreased from 76.95% at 30 °C to 42.21% at 70 °C, while undesirable disproportionation increased from 7.15% to 56.89% over the same temperature range. Although the O_3 + Mn/ZSM-5 system showed improved overall performance, NO_2^- oxidation efficiency still declined from 92.81% (30 °C) to 54.84% (70 °C), while disproportionation rose from 1.89% to 44.86%. Comparative analysis of the two systems revealed that the Mn/ZSM-5 catalyst significantly reduced the temperature sensitivity of the reaction system. When the temperature increased to 60 °C, the O_3 + Mn/ZSM-5 system maintained NO_2^- oxidation efficiency above 75%. This demonstrated that the Mn/ZSM-5 catalyst can further enhance the selectivity of NO_2^- oxidation pathway while effectively suppressing the disproportionation reaction. The superior catalytic performance and stability of Mn/ZSM-5 effectively broaden the optimal temperature operating window for this process.

From the perspectives of reaction thermodynamics and kinetics, conventional oxidation reactions typically intensify with increasing temperature, primarily due to the temperature-dependent mechanism of chemical reaction rates. However, in our system, the oxidation efficiency of NO_2^- decreased with rising temperature rather than improved. This observation suggested that although intensified ionic movement of NO_2^- occurred in the liquid phase, effective collisions with oxidants were limited. Simultaneously, increased temperature enhanced collision probabilities between NO_2^- and H^+, which subsequently promoted an undesirable disproportionation reaction. The competitive relationship between oxidation and disproportionation pathways in the liquid phase ultimately suppressed NO_2^- oxidation efficiency.

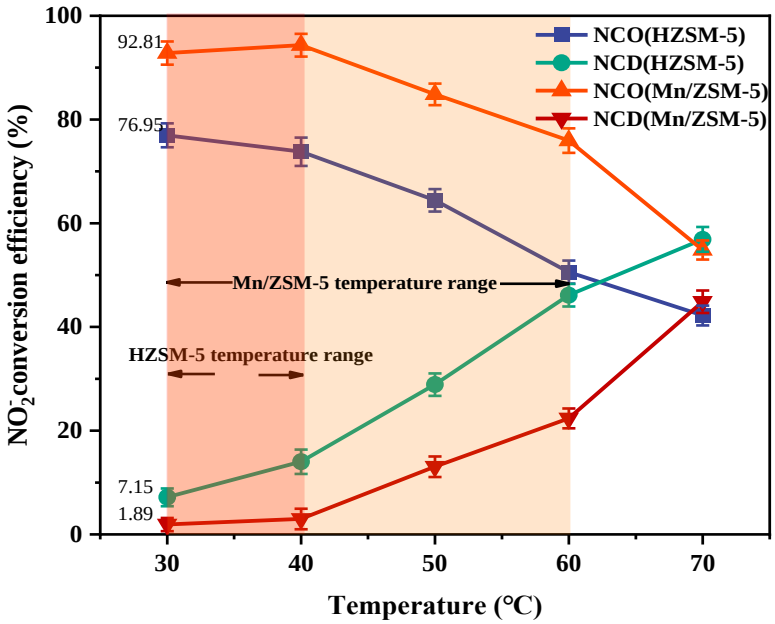

Figure 6. Effect of reaction temperature on NO_2^- oxidation efficiency and conversion pathways.

3.3.2. Effect of Initial Liquid pH Value

The effect of initial liquid pH on NO_2^- oxidation efficiency and conversion pathways is illustrated in Figure 7. Experimental data demonstrated that the initial pH played a pivotal regulatory role in both the oxidation efficiency and reaction pathways of NO_2^-. Under acidic conditions (initial pH = 4), the O_3 + HZSM-5 system achieved 73.79% NO_2^- oxidation efficiency. However, when the pH increased to six, the efficiency sharply decreased to 32.09%. This phenomenon correlated with the catalyst's zero point of charge (ZPC) [76,77]. When pH < ZPC, positively charged sites form on the catalyst surface, enabling NO_2^- enrichment at the interface. Conversely, when pH > ZPC, electrostatic repulsion occurred between the negatively charged Mn/ZSM-5 surface and NO_2^- anions, significantly inhibiting surface adsorption and consequently reducing NO_2^- oxidation efficiency. Further analysis revealed that pH also critically affected ozone stability. Molecular ozone concentration markedly decreased under alkaline conditions, while remaining nearly undecomposed in acidic media [78,79]. These combined factors accounted for the observed decline in NO_2^- oxidation efficiency in the O_3 + HZSM-5 system. According to heterogeneous catalytic ozonation theory, solution pH served as a primary determinant of ozonation efficiency by altering reaction kinetics and pathways. At low pH, direct ozonation dominated and demonstrated selectivity, whereas alkaline conditions favored indirect pathways involving radical chain reactions [70,80]. Therefore, NO_2^- oxidation in the O_3 + HZSM-5 system predominantly proceeded through direct ozonation mechanisms.

As shown in Figure 7, the O_3 + Mn/ZSM-5 system achieved 94.33% NO_2^- oxidation efficiency at pH = 4. When the pH was increased to six, the Mn/ZSM-5 catalyst still maintained 75.73% oxidation efficiency. Remarkably, even under alkaline conditions, the Mn/ZSM-5 catalyst demonstrated considerable oxidative performance. These results indicated that the superior NO_2^- oxidation in the O_3 + Mn/ZSM-5 system arose from the synergistic effect between direct ozonation and radical chain reactions. This phenomenon demonstrated that the Mn/ZSM-5 catalyst possessed superior pH adaptability, where the incorporation of active Mn species effectively broadened the operational pH window of the catalytic system. The doping of Mn species not only enhanced the acid stability of the zeolite support but also created Mn^{3+}/Mn^{4+} active sites that facilitated the directional adsorption and activation of ozone molecules on the catalyst surface. These active sites

lowered the activation energy for ozone decomposition into hydroxyl radicals, thereby maintaining efficient electron transfer between ozone and NO_2^- through coordination activation mechanisms even when elevated pH reduces surface protonation. From the perspective of interfacial reaction kinetics, these findings substantiated the exceptional structural stability and catalytic durability of Mn/ZSM-5 zeolite catalyst under varying pH conditions.

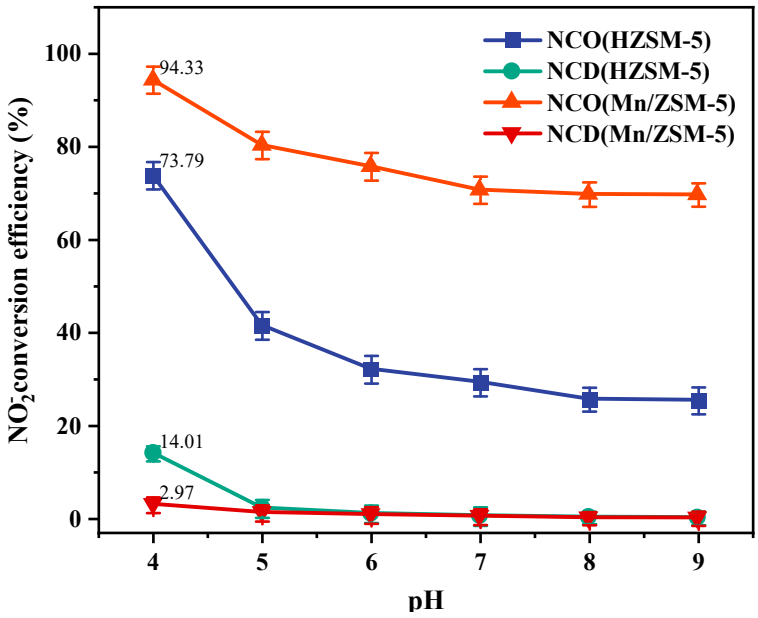

Figure 7. Effect of initial liquid pH on NO_2^- oxidation efficiency and conversion pathways.

3.3.3. Effect of Oxidant Concentration

The effect of ozone concentration on the heterogeneous catalytic oxidation of NO_2^- was investigated in Figure 8. Kinetic experimental data revealed that in the O_3 + Mn/ZSM-5 catalytic system, NO_2^- oxidation efficiency exhibited a significant transition from 79.45% to 94.33% as ozone concentration increased from 50 ppm to 100 ppm, following pseudo-first order reaction kinetics. When the ozone concentration was further elevated to 150 ppm, the oxidation efficiency demonstrated marginal effect characteristics with only a 0.5% enhancement, and upon exceeding 150 ppm, the NO_2^- oxidation efficiency entered a stable plateau region at 95%, displaying distinct mass transfer limitation features. Synchronous monitoring indicated that the disproportionation side reaction rate stabilized at 2.5% when ozone concentration reached 150 ppm, showing significant correlation with the oxidation efficiency stagnation observed in the high ozone concentration range.

Comparative analysis of different catalytic systems revealed that when the ozone concentration decreased from 100 ppm to 50 ppm, the NO_2^- oxidation efficiency in the O_3 + HZSM-5 system significantly dropped from 73.79% to 50.71%. This demonstrated that ozone concentration served as a critical parameter governing the catalytic oxidation performance. Remarkably, under identical ozone concentration reduction, the O_3 + Mn/ZSM-5 system maintained ~ 80% NO_2^- oxidation efficiency, indicating that the synergistic effect between Mn species and the zeolite support substantially enhances ozone utilization efficiency. The Mn/ZSM-5 system achieved comparable oxidation performance with lower ozone consumption, demonstrating better economic feasibility. The observed limitation in NO_2^- oxidation efficiency at elevated ozone concentrations can be mechanistically explained by interfacial regulation phenomena in the heterogeneous catalytic system: Mn active sites reached adsorption–desorption equilibrium under high ozone concentrations, rendering excess ozone ineffective for surface catalytic cycles, while simultaneous mass

transfer limitations created diffusion barriers for NO_2^- migration from the liquid phase to catalytic interfaces. The unconverted NO_2^- remaining in the liquid phase consequently underwent competitive disproportionation reactions with H^+, collectively constraining the overall oxidation efficiency through these parallel pathways.

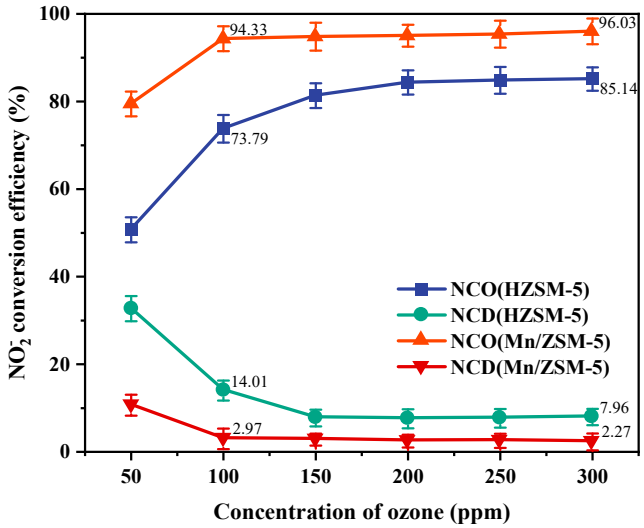

Figure 8. Effect of ozone concentration on NO_2^- oxidation efficiency and conversion pathways.

The effect of oxygen concentration on NO_2^- oxidation efficiency was also considered, as shown in Figure 9. It was noteworthy that the single-ozone system maintained only ~60% oxidation efficiency while exhibiting a disproportionation rate of 20%. It demonstrated that the sole ozone oxidation pathway was constrained by mass transfer limitations arising from low oxidant concentration, and ozone alone cannot effectively achieve high-efficiency NO_2^- oxidation. When ozone and oxygen coexist, the NO_2^- oxidation efficiency significantly improved with concomitant suppression of the disproportionation reaction. This phenomenon can be attributed to synergistic effects in the ozone-oxygen dual-oxidant system: (1) molecular oxygen contributes partially to NO_2^- oxidation; (2) competitive adsorption of oxygen inhibits ineffective ozone decomposition on the catalyst surface; and (3) the strong oxidative potential of ozone enhances interfacial electron transfer efficiency, thereby shifting the reaction pathway selectivity from disproportionation (Equation (1)) toward complete oxidation ($NO_2^- \rightarrow NO_3^-$).

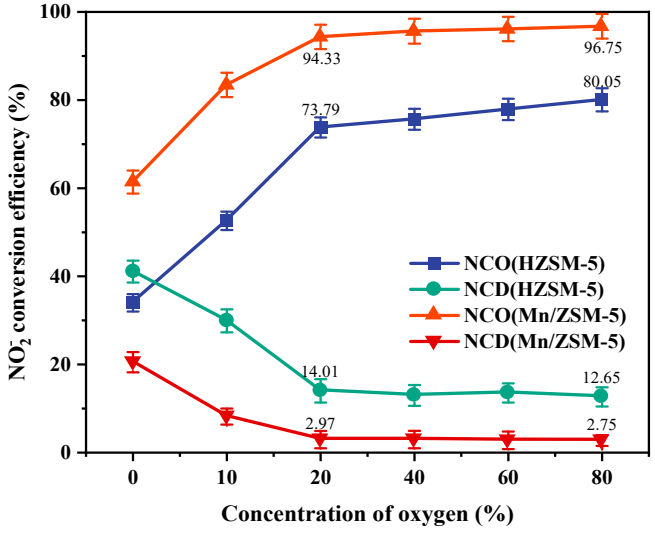

Figure 9. Effect of oxygen concentration on NO_2^- oxidation efficiency and conversion pathways.

3.4. Mechanisms of Catalytic Ozonation on Mn/ZSM-5 Zeolite Catalyst

Existing literature studies indicate that three possible scenarios may occur in heterogeneous catalytic ozonation systems [81,82]:

(1) O_3 adsorbs on the catalyst surface and decomposes to form radicals, which subsequently react with NO_2^- in the solution.
(2) NO_2^- adsorbs on the catalyst and is then attacked by O_3 molecules or other reactive species.
(3) Both O_3 and NO_2^- adsorb on the catalyst surface and undergo direct reaction.

Results found that the reaction mechanisms of heterogeneous wet catalytic ozonation could be primarily categorized into two pathways: the direct molecular ozone oxidation pathway and the radical chain reaction pathway. Surface adsorption played a crucial role in heterogeneous catalytic ozonation processes. In the O_3 + Mn/ZSM-5 catalytic system, NO_2^- can react simultaneously with both ozone molecules and their derived radical species. It is worth emphasizing that under the acidic conditions employed in our experiments, ozone molecules exhibited high stability with a low tendency for self-decomposition into hydroxyl radicals. Particularly when ZSM-5 zeolite served as the catalyst, its surface acid sites demonstrate a negligible promotion effect on ozone decomposition for radical generation [41]. The introduction of Mn active species had been reported to significantly improve this situation [83]. Kinetic analysis of the experimental system revealed that NO_2^- underwent two competitive transformation pathways during the reaction: oxidation and disproportionation. The disproportionation reaction predominantly occurred in the bulk liquid phase, whereas the oxidation process was highly dependent on surface adsorption and active sites on the catalyst.

To elucidate the dominant mechanism of the O_3 + Mn/ZSM-5 catalytic system in the oxidation reaction, a radical identification experimental strategy was employed to analyze the contribution of reactive oxygen species. As shown in Figure 10, by selectively adding hydroxyl radical scavenger tert-butanol (TBA) and superoxide radical scavenger benzoquinone (BQ), the variations in reaction kinetics under different radical inhibition conditions were systematically compared. This approach enabled effective discrimination between the direct ozone oxidation pathway and the radical chain reaction pathway in the heterogeneous wet catalytic oxidation system. In the O_3 + HZSM-5 zeolite catalytic system, the introduction of TBA and BQ did not induce significant changes in either the NO_2^- oxidation efficiency or the reaction pathway. This observation confirmed that the oxidation reaction in the O_3 + HZSM-5 system followed a non-radical-mediated mechanism, where the direct interaction between NO_2^- and molecular ozone constituted the fundamental reaction pathway. The process was essentially characterized by direct electron transfer between NO_2^- and molecular ozone occurring on the catalyst surface.

Notably, in the O_3 + Mn/ZSM-5 system, the addition of TBA resulted in a decrease in NO_2^- oxidation efficiency from 94.33% to 73.38%, accompanied by an increase in the disproportionation ratio from 2.96% to 13.71%. These catalytic performance parameters approached those of the O_3 + HZSM-5 system. This demonstrated that the introduction of Mn active components promoted the generation of oxidative hydroxyl radicals (OH) in the reaction system, and ·OH played a crucial role in the deep ozonation of NO_2^-. When BQ was introduced, the NO_2^- oxidation efficiency remained at 93.74%, showing no significant difference from the system without radical scavengers. The addition of BQ caused no observable changes in either NO_2^- oxidation efficiency or reaction pathway. This indicated that the Mn active components did not facilitate the generation of superoxide radicals (O_2^-) in the reaction system. Therefore, the oxidation reaction in the O_3 + Mn/ZSM-5 heterogeneous wet catalytic oxidation system proceeded through a dual mechanism involving both the direct ozonation, as well as the reaction between NO_2^- and hydroxyl radicals.

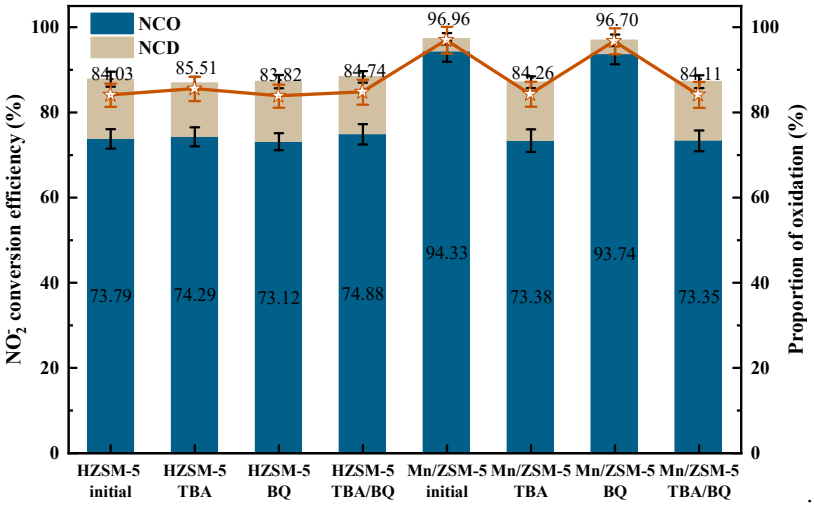

Figure 10. Effect of radical scavengers on NO_2^- oxidation efficiency and conversion pathways.

Based on comprehensive characterization and kinetic studies, this work proposed a mechanism for the heterogeneous wet catalytic oxidation in the O_3 + Mn/ZSM-5 system, as shown in Figure 11: The efficient catalytic oxidation of NO_2^- proceeded through a synergistic combination of direct ozonation and radical chain reactions. Under acidic conditions, NO_2^- preferentially adsorbed onto the acidic sites of Mn/ZSM-5 zeolite via electrostatic interactions, forming stable surface-adsorbed species. Molecular ozone underwent chemical adsorption on the catalyst surface, enabling direct oxidation of partially adsorbed NO_2^- species. Concurrently, ozone activation occurs at Mn^{3+}/Mn^{4+} active sites, generating highly reactive hydroxyl radicals (OH). These radical species subsequently participated in oxidation reactions with NO_2^- through interfacial diffusion, thereby enhancing the overall oxidation performance. Furthermore, the strong adsorption of NO_2^- by the Mn/ZSM-5 zeolite effectively suppressed its migration to the bulk liquid phase. Combined with the competitive mechanism between oxidation and disproportionation pathways, these factors collectively inhibited NO_2^- disproportionation in the liquid phase. This dual-path synergistic mechanism elucidated the intrinsic regulation principle of Mn/ZSM-5 catalysts in achieving reaction pathway optimization through controlled surface adsorption–oxidation processes.

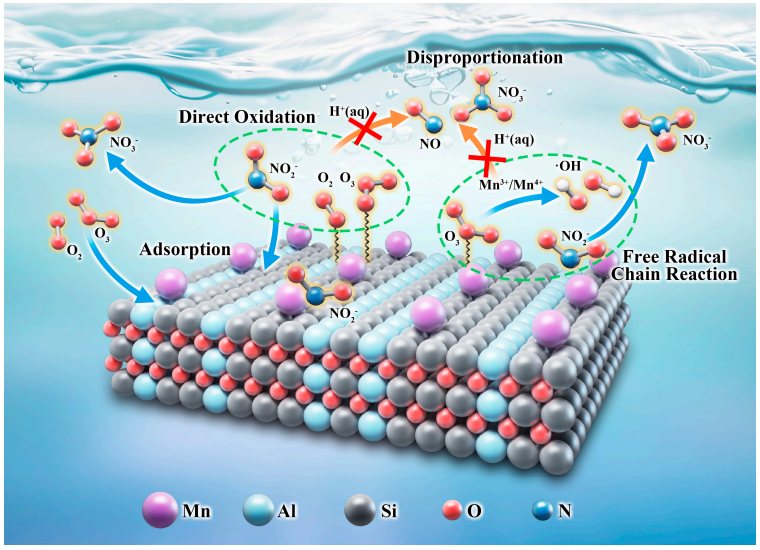

Figure 11. The mechanism for the heterogeneous wet catalytic oxidation of NO_2^- in O_3 + Mn/ZSM-5 system.

3.5. Effect of O_3 + Mn/ZSM-5 System on Ozone Oxidation Flue Gas Denitrification System

In this section, the synergistic treatment of flue gas pollutants and liquid-phase absorption byproduct NO_2^- was investigated by coupling the O_3 + Mn/ZSM-5 heterogeneous wet catalytic oxidation system with an ozone oxidation denitrification technology spray absorption system. The experiments were conducted using a designed wet scrubbing tower, with the following Group I–IV. The specific operating parameters are detailed in Table 2.

Table 2. The specific operating parameters of the spray absorption system.

Group	Total Gas Volume	O_3/NO	Catalyst	Catalyst Dosage
I	5 L/min	1.6	-	0 g/L
II	5 L/min	1.6	Mn/ZSM-5 (400)	1 g/L
III	5 L/min	1.6	Mn/ZSM-5 (400)	2 g/L
IV	5 L/min	1.6	Mn/ZSM-5 (400)	3 g/L

This study focused on investigating the impact of Mn/ZSM-5 zeolite catalyst introduction on both the flue gas pollutant removal efficiency and the operational stability of the spray absorption system. As shown in Figure 12, under an O_3/NO molar ratio of 1.6, the ozone oxidation denitrification system demonstrated excellent synergistic removal performance for NO_x/SO_2. Experimental data revealed that SO_2 was completely removed after oxidation–absorption treatment, while the overall NO_x removal efficiency remained consistently above 93%. Notably, comparative analysis between the blank control (Group I) and catalytic test groups (Groups II–IV) showed NO_x removal efficiency of 93.94%, 94.06%, 94.17%, and 94.49%, respectively, with no significant variation. This confirmed that the introduction of the Mn/ZSM-5 catalyst did not adversely affect the existing flue gas pollutant removal system. Further analysis indicated that, in the complex O_3-H_2O-NO_x-SO_2 multiphase system, the Mn/ZSM-5 catalyst neither altered the mass transfer and reaction kinetics of flue gas pollutants nor induced unfavorable phase transitions in the absorption liquid. This characteristic ensured the long-term stable operation of the spray absorption system.

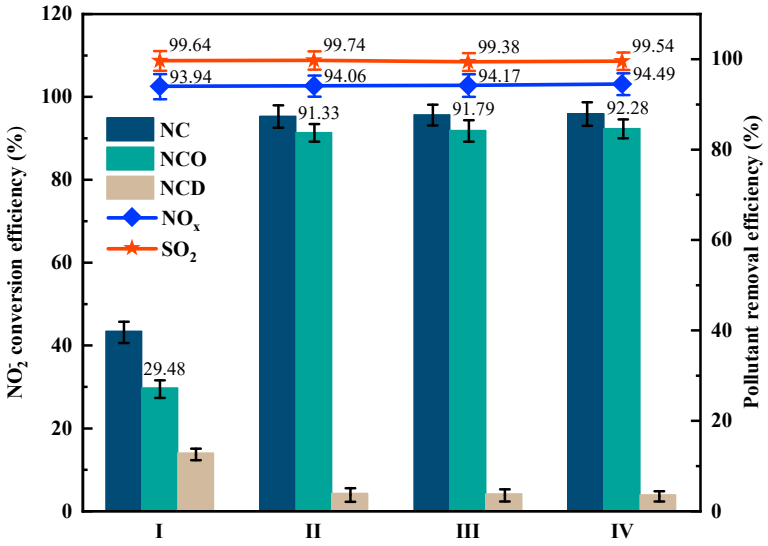

Figure 12. Effect of O_3 + Mn/ZSM-5 system on ozone oxidation flue gas denitrification system.

As shown in Figure 12, the NO_2^- oxidation efficiency remained merely 29.48% in the blank control group (Group I) without catalyst addition, while the catalytic systems exhibited remarkable NO_2^- oxidation enhancement effects. In Group II with 1 g/L Mn/ZSM-5

dosage, the total NO_2^- removal efficiency exceeded 95%, comprising 91.33% oxidation efficiency and 3.93% disproportionation rate. Groups III and IV showed similar performance to Group II. These results confirmed that the dual-path synergistic catalytic mechanism established by O_3 + Mn/ZSM-5 significantly enhanced NO_2^- oxidation efficiency in the absorption slurry. This process successfully reduced the environmental risk of denitrification byproduct nitrite by 1–2 orders of magnitude while maintaining >90% synergistic NO_x/SO_2 removal efficiency. This validated the catalytic performance of Mn/ZSM-5 and provided critical technical parameters for the green upgrading of wet flue gas desulfurization and denitrification processes.

4. Conclusions

This study developed a Mn-modified ZSM-5 zeolite catalyst. By establishing an O_3 + Mn/ZSM-5 heterogeneous wet catalytic oxidation system, efficient resource utilization of nitrite in denitrification wastewater could be achieved. The main conclusions are as follows:

(1) A significant structure–activity relationship existed between the SiO_2/Al_2O_3 ratio of Mn/ZSM-5 zeolite and its catalytic oxidation capability. The Mn/ZSM-5 (SiO_2/Al_2O_3 = 400) catalyst achieved an exceptional NO_2^- oxidation efficiency of 94.33%, which could be attributed to its optimal physicochemical properties, including the largest specific surface area, enhanced adsorption capacity, abundant surface Mn^{3+}/Mn^{4+} species, hydroxyl oxygen groups, and chemisorbed oxygen, which collectively contributed to remarkable improvements in both NO_2^- oxidation selectivity and catalytic activity. Repeated testing confirmed the outstanding structural stability and catalytic durability of Mn/ZSM-5, maintaining over 93% oxidation efficiency after multiple prolonged reaction cycles.

(2) The oxidation efficiency and conversion pathways of NO_2^- were governed by several key operational parameters, including reaction temperature, initial pH, catalyst dosage, and oxidant concentration. Compared with HZSM-5, the Mn/ZSM-5 catalyst demonstrated superior environmental adaptability and catalytic stability, effectively broadening the optimal operational windows for both temperature and pH in the catalytic oxidation process. The synergistic effect between Mn species and the zeolite support significantly enhanced ozone utilization efficiency, enabling the O_3 + Mn/ZSM-5 system to achieve comparable oxidation performance with substantially reduced ozone consumption, thereby improving overall economics. Furthermore, the combined use of oxygen and ozone proved more effective in promoting NO_2^- oxidation than ozone alone.

(3) In the O_3 + Mn/ZSM-5 heterogeneous wet catalytic oxidation system, the highly efficient catalytic oxidation of NO_2^- followed a dual-path reaction mechanism involving the synergistic combination of direct ozonation and radical chain reactions. Under acidic conditions, NO_2^- preferentially adsorbed onto the acidic sites of Mn/ZSM-5 zeolite via electrostatic interactions, forming stable surface-adsorbed species. Molecular ozone underwent chemical adsorption on the catalyst surface, enabling direct oxidation of partially adsorbed NO_2^- species. Concurrently, ozone activation occurred at the Mn^{3+}/Mn^{4+} active sites, generating highly reactive hydroxyl radicals (OH). These radical species subsequently participated in oxidation reactions with NO_2^- through interfacial diffusion, thereby enhancing the overall oxidation performance.

(4) The O_3 + Mn/ZSM-5 system demonstrated excellent compatibility with existing spray absorption systems for multi-pollutant removal, requiring no installation of additional liquid-phase byproduct treatment facilities. The introduction of the Mn/ZSM-5 catalyst would not affect the long-term operational stability of both the flue gas

purification system and spray absorption unit. Under conditions ensuring effective removal of flue gas pollutants, the O_3 + Mn/ZSM-5 system achieved 91.33% NO_2^- oxidation efficiency, providing critical technical parameters for the green upgrading of wet flue gas desulfurization and denitrification processes.

Supplementary Materials: The following supporting information can be downloaded at: https://www.mdpi.com/article/10.3390/pr13082387/s1, Figure S1: N2 adsorption-desorption isotherms and distribution curves of pore size of Mn/ZSM-5 catalysts; Figure S2: XRD patterns of Mn/ZSM-5 catalysts with different SiO_2/Al_2O_3 ratio; Figure S3. XPS spectra of (a) Mn $2p_{3/2}$ and (b) O 1s for Mn/ZSM-5 catalysts: (I) Mn/ZSM-5(21), (II) Mn/ZSM-5 (85), (III) Mn/ZSM-5 (200), (IV) Mn/ZSM-5 (300), (V) Mn/ZSM-5 (400); Table S1: Textual properties of Mn/ZSM-5 catalysts. Table S2: XPS results of Mn/ZSM catalysts.

Author Contributions: Data curation, Y.Z. (Yiwei Zhang); investigation, Y.Z. (Yiwei Zhang) and Y.S.; methodology, Y.Z. (Yiwei Zhang), Y.Z. (Yanqun Zhu), W.W. and Z.W.; project administration, Z.W.; resources, Z.W.; supervision, Y.Z. (Yanqun Zhu), Y.H. and Z.W.; validation, Y.Z. (Yiwei Zhang); visualization, Y.Z. (Yiwei Zhang); writing—original draft, Y.Z. (Yiwei Zhang); writing—review & editing, Y.Z. (Yanqun Zhu), W.W., Y.H. and Z.W. All authors have read and agreed to the published version of the manuscript.

Funding: This work was supported by the "Pioneer" and "Leading Goose" R&D Program of Zhejiang (2023C03126), the National Natural Science Foundation of China (52125605), and the Fundamental Research Funds for the Central Universities (2022ZFJH04).

Data Availability Statement: The original contributions presented in this study are included in the article/Supplementary Materials. Further inquiries can be directed to the corresponding authors.

Conflicts of Interest: The authors declare no conflicts of interest. The funders had no role in the design of the study; in the collection, analysis, or interpretation of data; in the writing of the manuscript, or in the decision to publish the results.

References

1. Sun, Y.; Zwolińska, E.; Chmielewski, A.G. Abatement technologies for high concentrations of NO_x and SO_2 removal from exhaust gases: A review. *Crit. Rev. Environ. Sci. Technol.* **2016**, *46*, 119–142. [CrossRef]
2. Ma, J.; Xu, X.; Zhao, C.; Yan, P. A review of atmospheric chemistry research in China: Photochemical smog, haze pollution, and gas-aerosol interactions. *Adv. Atmos. Sci.* **2012**, *29*, 1006–1026. [CrossRef]
3. Goldberg, D.L.; Lu, Z.; Streets, D.G.; Foy, D.B.; Griffin, D.; Mclinden, C.A.; Lamsal, L.N.; Krotkov, N.A.; Eskes, H. Enhanced Capabilities of TROPOMI NO_2: Estimating NO_x from North American Cities and Power Plants. *Environ. Sci. Technol.* **2019**, *53*, 12594–12601. [CrossRef]
4. Ji, Y.; Gao, F.; Wu, Z.; Li, L.; Li, D.; Zhang, H.; Zhang, Y.; Gao, J.; Bai, Y.; Li, H. A review of atmospheric benzene homologues in China: Characterization, health risk assessment, source identification and countermeasures. *J. Environ. Sci.* **2020**, *95*, 225–239. [CrossRef]
5. Shao, J.; Xu, C.; Wang, Z.; Zhang, J.; Wang, R.; He, Y.; Cen, K. NO_x reduction in a 130 t/h biomass-fired circulating fluid bed boiler using coupled ozonation and wet absorption technology. *Ind. Eng. Chem. Res.* **2019**, *58*, 18134–18140. [CrossRef]
6. Liu, P.; Zhang, Y.; Ma, X.; Xu, C.; He, Y.; Zhu, Y.; Alegria, E.C.B.A.; Wang, Z.; Pombeiro, A.J.L. Simultaneous Removal of Multipollutants (VOCs/NO/SO_2) by Catalytic Ozonation Coupled with Wet Scrubbing Technology: From the Laboratory to Industrial Testing. *Ind. Eng. Chem. Res.* **2024**, *63*, 8610–8621. [CrossRef]
7. Lin, F.; Wang, Z.; Ma, Q.; He, Y.; Whiddon, R.; Zhu, Y.; Liu, J. N_2O_5 Formation Mechanism during the Ozone-Based Low-Temperature Oxidation deNO_x Process. *Energy Fuels* **2016**, *30*, 5101–5107. [CrossRef]
8. Shao, J.; Yang, Y.; Whiddon, R.; Wang, Z.; Lin, F.; He, Y.; Kumar, S.; Cen, K. Investigation of NO removal with ozone deep oxidation in Na_2CO_3 solution. *Energy Fuels* **2019**, *33*, 4454–4461. [CrossRef]
9. Wang, Z.; Zhou, J.; Zhu, Y.; Wen, Z.; Liu, J.; Cen, K. Simultaneous removal of NO_x, SO_2 and Hg in nitrogen flow in a narrow reactor by ozone injection: Experimental results. *Fuel Process. Technol.* **2007**, *88*, 817–823. [CrossRef]
10. Tang, H.; He, Y.; Lin, F.; Zhu, Y.; Duan, Y.; Wang, Z. Simultaneous catalytic ozonation of NO and dichloromethane on Mn/H-ZSM-5 catalysts: Interaction effect and mechanism. *Proc. Combust. Inst.* **2023**, *39*, 4387–4397. [CrossRef]

11. Lin, F.; Wang, Z.; Zhang, Z.; He, Y.; Zhu, Y.; Shao, J.; Yuan, D.; Chen, G.; Cen, K. Flue gas treatment with ozone oxidation: An overview on NO_x, organic pollutants, and mercury. *Chem. Eng. J.* **2020**, *382*, 123030. [CrossRef]
12. Chang, F.; Lei, B.; Yang, C.; Wang, J.; Hu, X. Ultra-stable $Bi_4O_5Br_2/Bi_2S_3$ n-p heterojunctions induced simultaneous generation of radicals OH and O_2^- and NO conversion to nitrate/nitrite species with high selectivity under visible light. *Chem. Eng. J.* **2021**, *413*, 127443. [CrossRef]
13. Guo, L.; Han, C.; Zhang, S.; Zhong, Q.; Ding, J.; Zhang, B.; Zeng, Y. Enhancement effects of O_2^- and OH radicals on NO_x removal in the presence of SO_2 by using an O_3/H_2O_2 AOP system with inadequate O_3 (O_3/NO molar ratio = 0.5). *Fuel* **2018**, *233*, 769–777. [CrossRef]
14. Wu, Q.; Sun, C.; Wang, H.; Wang, T.; Wang, Y.; Wu, Z. The role and mechanism of triethanolamine in simultaneous absorption of NO_x and SO_2 by magnesia slurry combined with ozone gas-phase oxidation. *Chem. Eng. J.* **2018**, *341*, 157–163. [CrossRef]
15. Kim, H.; Lim, T.J.; Eom, H.H.; Kim, Y.J.; Kim, K.; Lee, J.W. Reconstructed fluorine doped perovskites for electrocatalytic urea production through reaction pathways with CO_2 and nitrate ions. *Appl. Catal. B Environ. Energy* **2025**, *365*, 124974. [CrossRef]
16. Jiang, H.; Li, T.; Gao, Y.; Fan, J.; Gan, D.; Yuan, S.; Hong, L.; Feng, Y.; Sun, J.; Song, Q.; et al. Sustainable ammonia synthesis: Opportunities for electrocatalytic nitrate reduction. *J. Energy Chem.* **2025**, *105*, 630–668. [CrossRef]
17. Aridi, R.; Yehya, A. Review on the sustainability of phase-change materials used in buildings. *Energy Convers. Manag. X* **2022**, *15*, 100237. [CrossRef]
18. Dungel, P.; Weidinger, A.; Wagner, C.; Redl, H.; Kozlov, A. Effects of nitrite on hepatocytes damaged by hypoxia/reoxygenation (H/R) in various in vitro models. *Nitric Oxide* **2011**, *24*, S34. [CrossRef]
19. Tau, P.; Nyokong, T. Electrocatalytic activity of arylthio tetra-substituted oxotitanium(IV) phthalocyanines towards the oxidation of nitrite. *Electrochim. Acta* **2007**, *52*, 4547–4553. [CrossRef]
20. Picetti, R.; Deeney, M.; Pastorino, S.; Miller, M.R.; Shah, A.; Leon, D.A.; Dangour, A.D.; Green, R. Nitrate and nitrite contamination in drinking water and cancer risk: A systematic review with meta-analysis. *Environ. Res.* **2022**, *210*, 112988. [CrossRef]
21. Zhang, Y.; Wang, Z.; He, Y.; Zhu, Y.; Liu, J. Experimental study on three additives used for the removal of nitrite, a byproduct of ozone oxidation denitration technology. *Environ. Technol. Innov.* **2023**, *32*, 103236. [CrossRef]
22. Lim, J.H.; Goh, K.; Ng, D.Y.F.; Jiang, X.; Chuah, C.Y.; Chew, J.W.; Wang, R. Alternating spin-and-spray electrospun scaffold membranes with fractionated MIL-101(Cr) adsorbent for high-performance single-pass dye adsorption process. *Chem. Eng. J.* **2022**, *450*, 137963. [CrossRef]
23. Zhao, Q.; Chen, K.; Li, J.; Sun, S.; Jia, T.; Huang, Y.; Peng, Y.; Zhang, L. Pilot-scale evaluation of partial denitrification/anammox on nitrogen removal from low COD/N real sewage based on a modified process. *Bioresour. Technol.* **2021**, *338*, 125580. [CrossRef]
24. Neşe, Ö.; TEnnil, K. A kinetic study of nitrite adsorption onto sepiolite and powdered activated carbon. *Desalination* **2008**, *223*, 174–179. [CrossRef]
25. Ahn, J.; Choo, K.; Park, H. Reverse osmosis membrane treatment of acidic etchant wastewater: Effect of neutralization and polyelectrolyte coating on nitrate removal. *J. Membr. Sci.* **2008**, *310*, 296–302. [CrossRef]
26. López, J.; Gibert, O.; Cortina, J.L. Integration of membrane technologies to enhance the sustainability in the treatment of metal-containing acidic liquid wastes. An overview. *Sep. Purif. Technol.* **2021**, *265*, 118485. [CrossRef]
27. Martínez, J.; Ortiz, A.; Ortiz, I. State-of-the-art and perspectives of the catalytic and electrocatalytic reduction of aqueous nitrates. *Appl. Catal. B Environ.* **2017**, *207*, 42–59. [CrossRef]
28. Marchesini, F.A.; Gutierrez, L.B.; Querini, C.A.; Miró, E.E. Pt, In and Pd, In catalysts for the hydrogenation of nitrates and nitrites in water. FTIR characterization and reaction studies. *Chem. Eng. J.* **2010**, *159*, 203–211. [CrossRef]
29. Guo, Z.; Zheng, Z.; Gu, C.; Zheng, Y. Gamma irradiation-induced removal of low-concentration nitrite in aqueous solution. *Radiat. Phys. Chem.* **2008**, *77*, 702–707. [CrossRef]
30. Samatya, S.; Kabay, N.; Yüksel, Ü.; Arda, M.; Yüksel, M. Removal of nitrate from aqueous solution by nitrate selective ion exchange resins. *React. Funct. Polym.* **2006**, *66*, 1206–1214. [CrossRef]
31. Bian, X.; Wu, Y.; Li, J.; Yin, M.; Li, D.; Pei, H.; Chang, S.; Guo, W. Effect of dissolved oxygen on high C/N wastewater treatment in moving bed biofilm reactors based on heterotrophic nitrification and aerobic denitrification: Nitrogen removal performance and potential mechanisms. *Bioresour. Technol.* **2022**, *365*, 128147. [CrossRef]
32. Hao, Z.; Ali, A.; Ren, Y.; Su, J.; Wang, Z. A mechanistic review on aerobic denitrification for nitrogen removal in water treatment. *Sci. Total Environ.* **2022**, *847*, 157452. [CrossRef]
33. Zhang, H.; Li, S.; Zhang, C.; Ren, X.; Zhou, M. A critical review of ozone-based electrochemical advanced oxidation processes for water treatment: Fundamentals, stability evaluation, and application. *Chemosphere* **2024**, *365*, 143330. [CrossRef]
34. Jiang, Y.; Gao, K.; Chen, T.; Xiong, Y.; Li, Y.; Addisu, A.; Pillai, S.C.; Dionysiou, D.D.; Wang, D. Regulating the generation of singlet oxygen ($^1O_2$) in Advanced oxidation processes by catalyst design for water treatment. *Chem. Eng. J.* **2024**, *500*, 156532. [CrossRef]
35. Sushma Kumari, M.; Saroha, A.K. Performance of various catalysts on treatment of refractory pollutants in industrial wastewater by catalytic wet air oxidation: A review. *J. Environ. Manag.* **2018**, *228*, 169–188. [CrossRef]

36. Chen, J.; Tu, Y.; Shao, G.; Zhang, F.; Zhou, Z.; Tian, S.; Ren, Z. Catalytic ozonation performance of calcium-loaded catalyst (Ca-C/Al_2O_3) for effective treatment of high salt organic wastewater. *Sep. Purif. Technol.* **2022**, *301*, 121937. [CrossRef]
37. Gulde, R.; Clerc, B.; Rutsch, M.; Helbing, J.; Salhi, E.; Mcardell, C.S.; Gunten, V.U. Oxidation of 51 micropollutants during drinking water ozonation: Formation of transformation products and their fate during biological post-filtration. *Water Res.* **2021**, *207*, 117812. [CrossRef]
38. Graça, C.A.L.; Zema, R.; Orge, C.A.; Restivo, J.; Sousa, J.; Pereira, M.F.R.; Soares, O.S.G.P. Temperature and nitrogen-induced modification of activated carbons for efficient catalytic ozonation of salicylic acid as a model emerging pollutant. *J. Environ. Manag.* **2023**, *344*, 118639. [CrossRef]
39. You, N.; Deng, S.; He, H.; Hu, J. Ferromanganese oxide-functionalized TiO_2 for rapid catalytic ozonation of PPCPs through a coordinated oxidation process with adjusted composition and strengthened generation of reactive oxygen species. *Water Res.* **2024**, *258*, 121813. [CrossRef]
40. Qin, Y.; Yuan, R.; Luo, S.; Huang, H.; He, X. Catalytic ozonation process for treating coking biochemical wastewater based on an Fe-Mn/Al_2O_3 catalyst. *Colloids Surf. A Physicochem. Eng. Asp.* **2025**, *713*, 136478. [CrossRef]
41. Ikhlaq, A.; Brown, D.R.; Kasprzyk-Hordern, B. Catalytic ozonation for the removal of organic contaminants in water on ZSM-5 zeolites. *Appl. Catal. B Environ.* **2014**, *154*, 110–122. [CrossRef]
42. Xue, E.; Seshan, K.; Ross, J. Roles of supports, Pt loading and Pt dispersion in the oxidation of NO to NO_2 and of SO_2 to SO_3. *Appl. Catal. B Environ.* **1996**, *11*, 65–79. [CrossRef]
43. Chen, K.; Wang, H.; Luo, X.; Li, J.; Xu, Y.; Meng, Q.; He, H.; Xu, J.; Huang, G. Recent advances in high-performance Cu/SiO_2 catalysts for hydrogenation of dimethyl oxalate to ethylene glycol. *Chem. Eng. Sci.* **2025**, *313*, 121761. [CrossRef]
44. Lu, P.; Ye, L.; Yan, X.; Fang, P.; Chen, X.; Chen, D.; Cen, C. Impact of toluene poisoning on MnCe/HZSM-5 SCR catalyst. *Chem. Eng. J.* **2021**, *414*, 128838. [CrossRef]
45. Su, Y.; Fu, K.; Zheng, Y.; Ji, N.; Song, C.; Ma, D.; Lu, X.; Han, R.; Liu, Q. Catalytic oxidation of dichloromethane over Pt-Co/HZSM-5 catalyst: Synergistic effect of single-atom Pt, Co_3O_4, and HZSM-5. *Appl. Catal. B Environ.* **2021**, *288*, 119980. [CrossRef]
46. Yan, R.; Lin, S.; Li, Y.; Liu, W.; Mi, Y.; Tang, C.; Wang, L.; Wu, P.; Peng, H. Novel shielding and synergy effects of Mn-Ce oxides confined in mesoporous zeolite for low temperature selective catalytic reduction of NO_x with enhanced SO_2/H_2O tolerance. *J. Hazard. Mater.* **2020**, *396*, 122592. [CrossRef]
47. Yang, X.; Zeng, Z.; Li, Z.; Zhang, Y.; Mao, W.; Wang, Z.; Sun, X.; Li, K.; Wang, F.; Ning, P. Defect confinement in CuO/HZSM-5-T catalysts: A novel approach for enhancing stability in AsH_3 catalytic oxidation. *Fuel* **2025**, *381*, 133367. [CrossRef]
48. Tao, Y.; Kanoh, H.; Abrams, L.; Kaneko, K. Mesopore-Modified Zeolites: Preparation, Characterization, and Applications. *Chem. Rev.* **2006**, *106*, 896–910. [CrossRef]
49. Li, H.; Zhao, Y.; Ji, D.; Zhao, X.; Li, C.; Guo, P.; Li, G. Synthesis of hollow HZSM-5 zeolite-based catalysts and catalytic performance in MTA reaction. *Microporous Mesoporous Mater.* **2022**, *329*, 111546. [CrossRef]
50. Ogura, M. Towards Realization of a Micro- and Mesoporous Composite Silicate Catalyst. *Catal. Surv. Asia* **2008**, *12*, 16–27. [CrossRef]
51. Sun, Y.; Liu, P.; Wang, Z.; Tang, H.; He, Y.; Zhu, Y. Efficient catalytic ozonation of ethyl acetate over Cu-Mn catalysts: Further insights into the reaction mechanism. *Chem. Eng. J.* **2023**, *477*, 147282. [CrossRef]
52. Tu, Y.; Shao, G.; Zhang, W.; Chen, J.; Qu, Y.; Zhang, F.; Tian, S.; Zhou, Z.; Ren, Z. The degradation of printing and dyeing wastewater by manganese-based catalysts. *Sci. Total Environ.* **2022**, *828*, 154390. [CrossRef]
53. Jiang, Q.; Chen, S.; Xu, Z. Development and application of catalysts for catalytic ozonation of Cl-VOCs at low temperature: A comprehensive review. *Sep. Purif. Technol.* **2024**, *333*, 125882. [CrossRef]
54. Chen, G.; Wang, Z.; Lin, F.; Zhang, Z.; Yu, H.; Yan, B.; Wang, Z. Comparative investigation on catalytic ozonation of VOCs in different types over supported MnO_x catalysts. *J. Hazard. Mater.* **2020**, *391*, 122218. [CrossRef]
55. Lin, F.; Wang, Z.; Ma, Q.; Whiddon, R.; Zhu, Y.; Cen, K. Catalytic deep oxidation of NO by ozone over MnO_x loaded spherical alumina catalyst. *Appl. Catal. B Environ.* **2016**, *198*, 100–111. [CrossRef]
56. Lin, F.; Zhang, Z.; Xiang, L.; Zhang, L.; Cheng, Z.; Wang, Z.; Yan, B.; Chen, G. Efficient degradation of multiple Cl-VOCs by catalytic ozonation over MnO_x catalysts with different supports. *Chem. Eng. J.* **2022**, *435*, 134807. [CrossRef]
57. Shu, Y.; He, M.; Ji, J.; Huang, H.; Liu, S.; Leung, D.Y.C. Synergetic degradation of VOCs by vacuum ultraviolet photolysis and catalytic ozonation over Mn-xCe/ZSM-5. *J. Hazard. Mater.* **2019**, *364*, 770–779. [CrossRef]
58. Huang, H.; Huang, H.; Zhan, Y.; Liu, G.; Wang, X.; Lu, H.; Xiao, L.; Feng, Q.; Dennis, Y.C.L. Efficient degradation of gaseous benzene by VUV photolysis combined with ozone-assisted catalytic oxidation: Performance and mechanism. *Appl. Catal. B Environ.* **2016**, *186*, 62–68. [CrossRef]
59. Esmaeilirad, M.; Zabihi, M.; Shayegan, J.; Khorasheh, F. Oxidation of toluene in humid air by metal oxides supported on γ-alumina. *J. Hazard. Mater.* **2017**, *333*, 293–307. [CrossRef]

60. Du, C.; Lu, S.; Wang, Q.; Buekens, A.G.; Ni, M.; Debecker, D.P. A review on catalytic oxidation of chloroaromatics from flue gas. *Chem. Eng. J.* **2018**, *334*, 519–544. [CrossRef]
61. Yang, P.; Zuo, S.; Zhou, R. Synergistic catalytic effect of $(Ce, Cr)_xO_2$ and HZSM-5 for elimination of chlorinated organic pollutants. *Chem. Eng. J.* **2017**, *323*, 160–170. [CrossRef]
62. Peng, Y.; Si, W.; Li, J.; Crittenden, J.; Hao, J. Experimental and DFT studies on Sr-doped $LaMnO_3$ catalysts for NO_x storage and reduction. *Catal. Sci. Technol.* **2015**, *5*, 2478–2485. [CrossRef]
63. Yang, W.; Su, Z.A.; Xu, Z.; Yang, W.; Peng, Y.; Li, J. Comparative study of α-, β-, γ- and δ-MnO_2 on toluene oxidation: Oxygen vacancies and reaction intermediates. *Appl. Catal. B Environ.* **2020**, *260*, 118150. [CrossRef]
64. Gopi, T.; Swetha, G.; Chandra Shekar, S.; Ramakrishna, C.; Saini, B.; Krishna, R.; Rao, P.V.L. Catalytic decomposition of ozone on nanostructured potassium and proton containing δ-MnO_2 catalysts. *Catal. Commun.* **2017**, *92*, 51–55. [CrossRef]
65. Liu, Y.; Yang, W.; Zhang, P.; Zhang, J. Nitric acid-treated birnessite-type MnO_2: An efficient and hydrophobic material for humid ozone decomposition. *Appl. Surf. Sci.* **2018**, *442*, 640–649. [CrossRef]
66. Jia, J.; Zhang, P.; Chen, L. Catalytic decomposition of gaseous ozone over manganese dioxides with different crystal structures. *Appl. Catal. B Environ.* **2016**, *189*, 210–218. [CrossRef]
67. Lin, F.; Shao, J.; Tang, H.; Li, Y.; Wang, Z.; Chen, G.; Yuan, D.; Cen, K. Enhancement of NO oxidation activity and SO_2 resistance over $LaMnO_{3+\delta}$ perovskites catalysts with metal substitution and acid treatment. *Appl. Surf. Sci.* **2019**, *479*, 234–246. [CrossRef]
68. Sun, M.; Li, W.; Zhang, B.; Cheng, G.; Lan, B.; Ye, F.; Zheng, Y.; Cheng, X.; Yu, L. Enhanced catalytic performance by oxygen vacancy and active interface originated from facile reduction of OMS-2. *Chem. Eng. J.* **2018**, *331*, 626–635. [CrossRef]
69. Wang, X.; Liu, Y.; Zhang, T.; Luo, Y.; Lan, Z.; Zhang, K.; Zuo, J.; Jiang, L.; Wang, R. Geometrical-Site-Dependent Catalytic Activity of Ordered Mesoporous Co-Based Spinel for Benzene Oxidation: In Situ DRIFTS Study Coupled with Raman and XAFS Spectroscopy. *ACS Catal.* **2017**, *7*, 1626–1636. [CrossRef]
70. Wang, J.; Xu, L. Advanced Oxidation Processes for Wastewater Treatment: Formation of Hydroxyl Radical and Application. *Crit. Rev. Environ. Sci. Technol.* **2012**, *42*, 251–325. [CrossRef]
71. Nawaz, F.; Cao, H.; Xie, Y.; Xiao, J.; Chen, Y.; Ghazi, Z.A. Selection of active phase of MnO_2 for catalytic ozonation of 4-nitrophenol. *Chemosphere* **2017**, *168*, 1457–1466. [CrossRef]
72. Costa, E.P.; Roccamante, M.; Amorim, C.C.; Oller, I.; Sánchez Pérez, J.A.; Malato, S. New trend on open solar photoreactors to treat micropollutants by photo-Fenton at circumneutral pH: Increasing optical pathway. *Chem. Eng. J.* **2020**, *385*, 123982. [CrossRef]
73. Ying, M.; Zhang, M.; Liu, Y.; Wu, Z. Ozone-assisted catalytic oxidation of aqueous nitrite ions on HZSM-5 zeolites. *Sci. Rep.* **2019**, *9*, 14322. [CrossRef]
74. Braschi, I.; Blasioli, S.; Buscaroli, E.; Montecchio, D.; Martucci, A. Physicochemical regeneration of high silica zeolite Y used to clean-up water polluted with sulfonamide antibiotics. *J. Environ. Sci.* **2016**, *43*, 302–312. [CrossRef]
75. Ma, S.; Zuo, X.; Xiong, J.; Ma, C.; Chen, Z. Feasibility of high silica ZSM-5 recovery by ozone with sulfamethoxazole removal from water. *J. Water Process Eng.* **2019**, *32*, 100956. [CrossRef]
76. Kasprzyk-Hordern, B.; Ziółek, M.; Nawrocki, J. Catalytic ozonation and methods of enhancing molecular ozone reactions in water treatment. *Appl. Catal. B Environ.* **2003**, *46*, 639–669. [CrossRef]
77. Nawrocki, J.; Kasprzyk-Hordern, B. The efficiency and mechanisms of catalytic ozonation. *Appl. Catal. B Environ.* **2010**, *99*, 27–42. [CrossRef]
78. Hu, J.; Wang, Q.; Wang, Y.; Wang, Q.; Li, Z. Enhanced ozonation of nitrobenzene in water using natural iron ores: Efficiencies, mechanisms and stability. *J. Water Process Eng.* **2024**, *61*, 105315. [CrossRef]
79. Yuan, X.; Qin, W.; Lei, X.; Sun, L.; Li, Q.; Li, D.; Xu, H.; Xia, D. Efficient enhancement of ozonation performance via ZVZ immobilized g-C_3N_4 towards superior oxidation of micropollutants. *Chemosphere* **2018**, *205*, 369–379. [CrossRef]
80. Ma, J.; Sui, M.; Zhang, T.; Guan, C. Effect of pH on MnO_x/GAC catalyzed ozonation for degradation of nitrobenzene. *Water Res.* **2005**, *39*, 779–786. [CrossRef]
81. Miklos, D.B.; Remy, C.; Jekel, M.; Linden, K.G.; Drewes, J.E.; Hübner, U. Evaluation of advanced oxidation processes for water and wastewater treatment—A critical review. *Water Res.* **2018**, *139*, 118–131. [CrossRef]
82. Wang, J.; Chen, H. Catalytic ozonation for water and wastewater treatment: Recent advances and perspective. *Sci. Total Environ.* **2020**, *704*, 135249. [CrossRef]
83. Liu, J.; Yuan, X.; Dong, H.; Sans, C. Progress in MnO_2/MnO_2-based materials catalytic ozonation process for water and wastewater treatment. *J. Environ. Manag.* **2025**, *383*, 125493. [CrossRef]